Int J Adv Manuf Technol (2016) 86:2139–2146
DOI 10.1007/s00170-015-8287-4

ORIGINAL ARTICLE

Improved predictions of the stability lobes for milling cutting operations of thin-wall components by considering ultra-miniature accelerometer mass effects

D. Olvera[1] · A. Elías-Zúñiga[1] · O. Martínez-Romero[1] · L. N. López de Lacalle[2] · H. Martínez-Alfaro[1] · H. R. Siller[1] · M. W. Pineda[3]

Received: 16 September 2015 / Accepted: 18 December 2015 / Published online: 18 January 2016

Abstract In this work, we study how the mass and the lightweight connecting cable of an ultra-miniature accelerometer sensor (ACC) influence the frequency response function (FRF) of thin-wall aluminum workpieces, and its influence over the stability analysis of the milling process. To address these effects, experimental FRF measurements were performed by using a noncontact laser Doppler vibrometer (LDV) system to compare its collected data with those obtained by using the ACC. To correlate the discrepancies observed between measurements, we have used the structural modification method and finite element simulations to quantify the accelerometer mass and its connecting cable effects. Then, we computed the stability lobes diagram by using the enhanced, multistage homotopy perturbation method (EMHPM) to determine stable cutting parameters. It was found that the predicted stability lobes agree well with experimental data if the structural modification method is used to compensate the accelerometer measurements. This methodology could help researches and machinist with limited access to LDV equipment to perform reliable experimental dynamic measurements in cases where the cable and accelerometer mass could affect data accuracy.

✉ A. Elías-Zúñiga
aelias@itesm.mx

[1] Center for Innovation in Design and Technology, Tecnológico de Monterrey, E. Garza Sada 2501 Sur, 64849 Monterrey, Nuevo León, Mexico

[2] Deparment of Mechanical Engineering, University of the Basque Country, Alameda de Urquijo s/n, 48013 Bilbao, Basque Country, Spain

[3] Polytec Inc., Irvine, CA 92618, USA

Keywords Thin-walled structures · Stability lobes · Accelerometer mass effect · Laser Doppler vibrometer · Homotopy perturbation method

1 Introduction

Chatter is a dynamic instability phenomenon that affect the quality of the machined part as well as the tool performance during milling [1], turning [2], among others machining operation processes performed by the automotive and the aeronautical industries. Therefore, these kinds of industries have focused their efforts on increasing dimensional accuracy in monolithic and thin-walled components to reduce manufacturing cost by introducing more accurate predictive physical models [3, 4], enhanced numerical methods [5–8], and high-technology experimental measurements [9, 10] to determine the optimum cutting parameters [11]. For instance, to machine thin wall parts that have a wall thickness of less than 5 mm and higher than 30 mm [12] requires peripheral milling operations that use a long, helical slender end mills to further reduce the part wall thickness. It is expected that the machining of these types of structures can experience regenerative lateral vibrations (chatter) for some cutting conditions which could result in poor surface finishing and lower productivity, as pointed out in [3, 13] and references cited therein. Furthermore, the collection of experimental data during the dynamic characterization of these low-rigidity structures could produce inaccurate measurements that can guide us to the misleading interpretation of the experimental data and of the theoretical simulations if the influence of the accelerometer mass is not taken into account during the frequency response function (FRF) measurements. For instance, Bravo and co-workers studied the effects of chatter on thin wall parts by considering the rigidities of the part according to the

relationship of the wall/tool interaction [14]. They developed three-dimensional stability lobe diagrams composed of spindle speed, machining stage, and maximum depth of cut. The FRF of the milled thin-walled components was obtained from impact tests, by using a micro-accelerometer (0.8 g) placed on the base. Later, Özsahin and co-workers analyzed the mass-loading effect on the tool FRF [15]. They obtained the FRF by tap testing, exciting the chain (spindle-holder-tool) with an impact hammer, and measured the vibration responses with an accelerometer (ACC) and a laser Doppler vibrometer (LDV), both at the tool's tip. They measured the FRF peak values for a carbide end mill of 12 mm diameter and 80 mm gauge length and found a shift of 167 Hz between both devices. They attributed this frequency shift to the accelerometer mass that influences directly the morphology of the predicted stability lobes diagram. Based on these findings, if one uses accelerometer devices to determine the modal parameter values needed to compute the cutting machine stability lobes, one could erroneously select machine parameter values that can lead to unstable machine operation instead of having a stable one. Therefore, the aim of this work focuses on studying the dynamic effects that the accelerometer's mass and its connecting cable could have during the experimental determination of the modal parameters of aluminum thin-walled workpieces, as well as their influence that these have on the prediction of the stability boundaries. We also investigate the discrepancies attained by comparing accelerometer and non-contact LDV measurements. The outcomes of this research work could be useful to perform accurate experimental dynamic measurements on thin-walled workpieces by using common accelerometers, which are more affordable than laser Doppler vibrometer.

2 Experimental determination of the modal parameters

To assess the influence of the accelerometer mass on the determination of the modal parameters of thin-walled structures, we used a Polytec compact laser vibrometer CLV-2534 that allows dynamic measurements without adding mass to the workpiece. In order to compare the mass loading effect over thin walls, we selected a Kistler type 8778A500M14 ultra-miniature accelerometer of 0.4 g and the Kistler Power Supply/Coupler 5134B. The M14 is a version of the ultra-miniature accelerometer with a twisted wire pair used to minimize the extra damping and mass of the cable in comparison with the standard ones. All tap tests were measured using the Polytec VibSoft-20 USB-based data acquisition system connected to an impulse force hammer Kistler 9722A. The data were acquired with the VibSoft software and then computed for displacement/force units.

The experimental measurements, using the ultra-miniature accelerometer, were performed on aluminum 7075 thin-wall workpieces of 1 mm thickness, 100 mm width, 50 mm height, and 15 g of wall mass (without considering the base mass). The blue solid line shown in Fig. 1a represents the collected FRF. We next used the laser vibrometer and performed an impact test on the workpiece to obtain its FRF without the accelerometer. The red solid line in Fig. 1a describes the corresponding FRF.

One can notice that there is a variation on the FRF functions obtained from both experimental procedures. In fact, experimental measurements performed by laser vibrometer captured the first and the third vibrational modes with peak values at 356 and 990 Hz, respectively. However, the

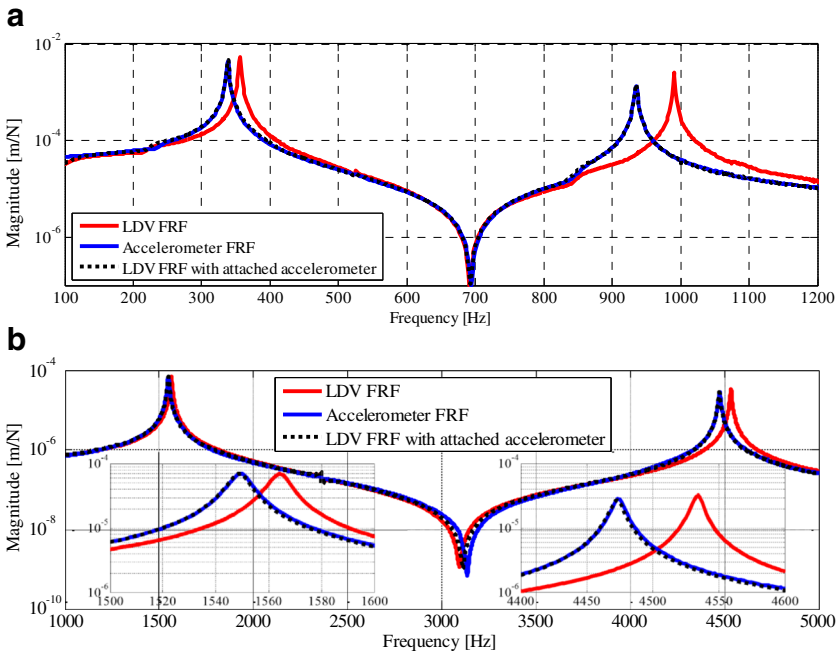

Fig. 1 FRF measurements in workpieces of nominal **a**) 1 mm and **b**) 5 mm wall thickness, with laser vibrometer without the accelerometer (*solid red line*), laser vibrometer with the accelerometer attached to the workpiece (*dashed black line*), and the accelerometer FRF measurements (*solid blue line*)

Table 1 Natural frequency values of the first lateral mode at different nominal wall thicknesses

Method	Measured workpiece wall thickness (mm)				
	1.05	1.96	2.92	3.87	4.84
	Natural frequency, Hz				
Euler-Bernoulli	343	645	956	1280	1570
LDV device	356	677	990	1308	1563
Accelerometer device	338	660	972	1288	1549
FEM without the accelerometer attached	365	673	979	1289	1554
FEM with the accelerometer attached	349	658	965	1275	1543

measurements performed with the accelerometer exhibit the first and third modes at 338 and 943 Hz. Notice that the second mode is suppressed due to the fact that the measurement position is in a node of the second mode. These differences on the recorded FRF measurements were also noticed during experimental tests because of the audible tone produced by the thin-wall workpiece. The same behavior was confirmed with 2, 3, 4, and 5 mm nominal thickness thin walls. Figure 1b shows that the shift on the values of the FRF obtained by these experimental procedures becomes smaller as the thickness of the wall increases.

In order to verify if the shift of the first peak modes could be due to the accelerometer mass, we performed experimental measurements by using the laser vibrometer while the accelerometer remains attached to the workpiece. The results are shown in Fig. 1 by the black dashed line. Notice that the FRF follows very closely experimental data collected with the accelerometer. This test confirms the influence that the accelerometer mass has on the measurement of the FRF values since it causes not only a shift of the first mode frequency value of about 5 % but it also changes the modal parameter values of the system. Therefore, it is assumed that the accelerometer's mass effects tend to decrease as the thickness of the workpiece wall increases. The FRF of the 5 mm nominal block was measured with the accelerometer attached to it and recorded a fundamental frequency peak value of 1549 Hz, while the fundamental frequency peak value obtained with the laser vibrometer device was 1563 Hz which represents a frequency shift of 0.9 %. Table 1 shows the recorded frequency peak values as the workpiece wall thickness changes.

3 Numerical simulations and experimental measurements

In order to evaluate the mass influence in modal analysis, we performed finite element method (FEM) numerical simulations by using the commercial computer package Abaqus 6.12-3. In this case, we used five workpieces of aluminum 7075 with 100 mm width and 50 mm height and the following manufacturing material property values: Poisson ratio of 0.33, a density value of 2800 kg/m^3, and Young modulus of 72 GPa. All numerical simulations were performed by assuming that the workpiece is fixed at its base. The thin-wall base dimensions were 18 mm width and 25 mm height, and the part was meshed by using tetrahedral elements. Figure 2 shows the first three vibrational modes of the workpiece (first bending, first twisting, second bending) with and without the 0.4 g of the accelerometer mass. From this analysis, it is clear that a 0.4 g extra mass changes the FRF by shifting the frequency peaks to different values, even for the second mode where the node coincides with the position of the accelerometer. The fundamental natural frequency values of the thin walls are listed in Table 1.

To perform experimental measurements, aluminum 7075 workpieces were machined with the nominal thickness values of 1, 2, 3, 4, and 5 mm; however, it is important to mention that the nominal thickness of the thin walls was not achieved due not only to the dynamic equilibrium between the cutting forces and the deflection of the part during the machining operation [12] but also to the total runout in the spindle axis-tool holder-tool chain. Then, the average thickness of each workpiece was measured after being machined and it was

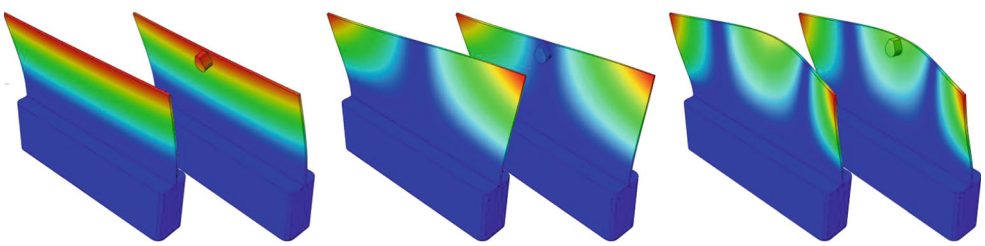

Fig. 2 FEM simulation results for a workpiece thickness of 1 mm (*left*) without and (*right*) with the accelerometer mass

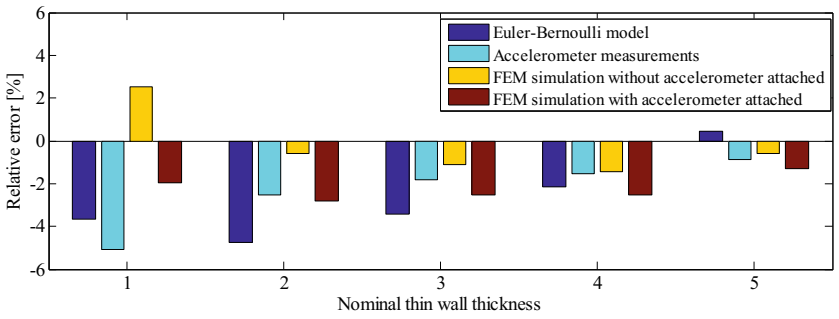

Fig. 3 Relative error compared with the first frequency measured with the laser vibrometer without the accelerometer

assumed as constant along the workpiece height to run the modal analysis by FEM. We next performed tap tests with the ultra-miniature accelerometer attached at the middle of the workpiece, at the distance of 5 mm under the upper edge of the thin wall in order to ensure accelerometer contact to the surface and symmetrical mass distribution.

To validate our experimental findings, we determine the theoretical beam natural frequency by using the equation of motion of the Euler-Bernoulli beam theory.

$$EI\frac{\partial^4 w}{dx^4}+\mu\frac{\partial^2 w}{dt^2}=0, \tag{1}$$

where E is the Young modulus, I is the inertia of the cross-sectional area of the beam, and μ represents the mass of the beam per unit length. In this case, Eq. (1) has an exact solution given as

$$\hat{w}=A_1\cosh(\beta x)+A_2\sinh(\beta x)+A_3\cos(\beta x)+A_4\sin(\beta x) \tag{2}$$

where $\beta=(\mu\omega^2/EI)^{1/4}$, A_1, A_2, A_3, and A_4 are integration constants that can be determined by using the system boundary conditions. However, the solution for the displacement is not unique since it depends on the vibration frequency of the system. In accordance with the end conditions of the thin-wall workpiece under consideration, it is clear that the boundary conditions are similar to those used in a cantilevered beam of length L that is fixed at $x=0$:

$$\begin{aligned}&\hat{w}_n=0,\frac{d\hat{w}_n}{dx}=0 \text{ at } x=0\\&\frac{d^2\hat{w}_n}{dx^2}=0,\ \frac{d^3\hat{w}_n}{dx^3} \text{ at } x=L\end{aligned} \tag{3}$$

Nontrivial solutions for Eq. (3) are found to exist if

$$\cosh(\beta_n L)\cos(\beta_n L)+1=0 \tag{4}$$

By numerically solving Eq. (4), we can get the vibration natural frequency of the system which is given as:

$$\omega_1=\beta_1{}^2\sqrt{\frac{EI}{\mu}}=\frac{3.515}{L^2}\sqrt{\frac{EI}{\mu}} \tag{5}$$

Figure 3 shows a comparison of the relative error among measurements, numerical simulations, and theoretical predictions, by considering the LDV system as the exact one. It is observed from Fig. 3 that theoretical predictions computed from Eq. (5) tend to underestimate the natural frequency experimental values at small workpiece thickness; however, these predictions become closer to the experimental data at increasing values of the wall thickness.

The FEM simulation results also confirm that by adding 0.4 g to the workpiece, the system dynamics behavior changes. This is because the added mass affects the mass density. For instance, for 1 mm of nominal thickness thin wall, the mass density of the part has the value of $\mu=0.295$ g/mm but if we add the effect of the ultra-miniature accelerometer mass then the added mass increases the mass density approximately $\mu_{acc}=0.1$ g/mm in a linear space of 5.8 mm, that represents a 34 % increase of the mass density. As a result, the first natural frequency is shifted −5.1 % with respect to the value computed without considering the accelerometer mass. Notice from Fig. 3 that for a 5 mm thin wall thickness, there is a −0.9 % shift value which confirms that the accelerometer mass effects become smaller at increasing workpiece thickness. Notice that

Fig. 4 *Left*: experimental setup for FRF measurements using LDV and accelerometer devices. *Right*: Kistler ultra-miniature accelerometer and Dytran mini-accelerometer attached to a thin wall of 1 mm thickness

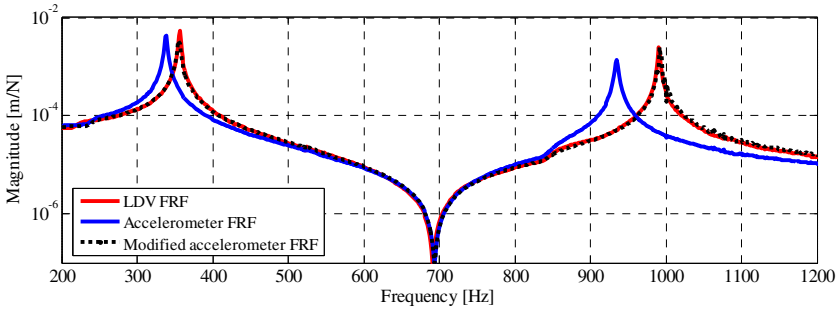

Fig. 5 FRF measurements with laser vibrometer (*red solid line*) and accelerometer (*solid blue line*) and modified FRF (*dashed black line*) for a subtracted 0.58 g extra mass

FEM simulations exhibit the same level of the accelerometer—LDV measurement errors (not more than 2.5 %), but take into consideration that the mechanical property values introduced into the FEM codes could have also discrepancies in comparison with real experimental ones.

4 Accelerometer mass effects compensation

In order to compensate the mass loading effects of the accelerometer when performing FRF experimental measurements on thin-wall workpieces, we followed the structural modification method suggested by H. N. Özgüven [16]. In this method, the FRF of the modified structure can be computed by coupling the original FRF, mass, stiffness, and damping properties of the system. Here, we use this approach to obtain the FRF of the workpiece when the mass of the accelerometer is attached to it. Let us consider the original system having a stiffness matrix **K**, a mass matrix **M**, and a structural damping matrix **H**. If we assume that the system is subjected to a harmonic force **F**, then the oscillation amplitudes **x** can be determined from the following expression:

$$\mathbf{x} = \left[\mathbf{K} - \omega^2\mathbf{M} + i\omega\mathbf{H}\right]^{-1}\mathbf{F}, \quad \text{where } i = \sqrt{-1}, \tag{6}$$

in which the receptance system matrix $\boldsymbol{\alpha}$ is defined as

$$\boldsymbol{\alpha} = \left[\mathbf{K} - \omega^2\mathbf{M} + i\omega\mathbf{H}\right]^{-1}. \tag{7}$$

Similarly, the receptance matrix of the modified system can be expressed as

$$\boldsymbol{\gamma} = \left[\mathbf{K} + \Delta\mathbf{K} - \omega^2(\mathbf{M} + \Delta\mathbf{M}) + i\omega(\mathbf{H} + \Delta\mathbf{H})\right]^{-1}, \tag{8}$$

where $\Delta\mathbf{K}$, $\Delta\mathbf{M}$, and $\Delta\mathbf{H}$ are the modified stiffness, mass, and damping matrices, respectively. Inverting both sides of Eqs. (7) and (8) and by combining the resulting equations yield

$$\boldsymbol{\gamma}^{-1} = \boldsymbol{\alpha}^{-1} + \mathbf{D}, \tag{9}$$

where **D** denotes the dynamic structural modification matrix which can be written as

$$\mathbf{D} = \Delta\mathbf{K} - \omega^2\Delta\mathbf{M} + i\omega\Delta\mathbf{H}. \tag{10}$$

As pointed out by Özgüven in [16], the above formulation for the modified receptance is appropriate when the structural modification is local. Then, the receptance matrix of the modified system, for coordinates where a modification exists, can be written as follows:

$$\gamma_{11} = (1 + \alpha_{11}D_{11})^{-1}\alpha_{11}, \tag{11}$$

where the subscript 11 refers to the modified region of the structure (driving point function of the upper edge of thin wall). This formulation reduces the order of the matrix that must be inverted. Notice that in the accelerometer's measurements, the modification on the assembly consists on only the mass of the accelerometer, and since the effect of the mass on the displacement-to-force receptance must be estimated, then the modification matrix must have the element $D_{11}=\Delta m_{acc}=-\omega^2 m_{acc}$, where m_{acc} is the mass of the accelerometer and ω represents the excitation frequency. Therefore, for the thin wall-vise assembly (*TWV*), the FRF can be written as

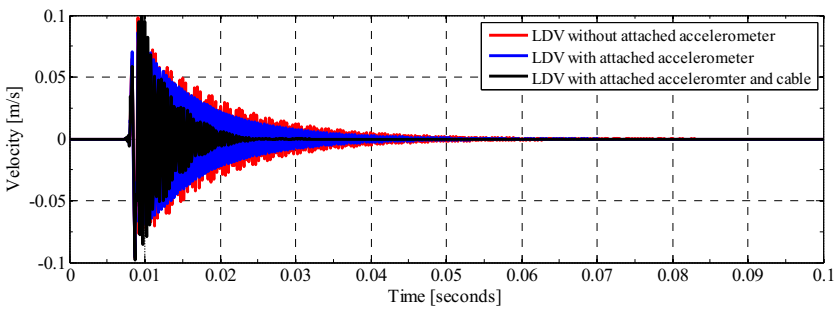

Fig. 6 Time domain vibrations of a 4.8 mm thick thin wall

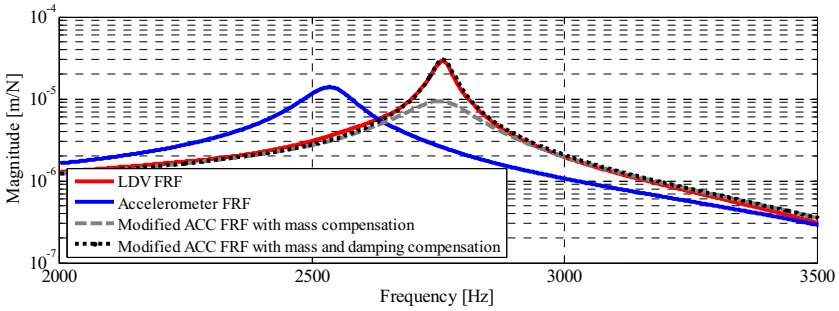

Fig. 7 FRF measurements with laser vibrometer (*solid red line*) and accelerometer (*solid blue line*), modified accelerometer FRF with mass compensation (*dashed black line*), modified accelerometer FRF with mass and damping compensation (*dotted black line*)

$$TWV_{11}^{m} = \frac{TWV_{11}^{um}}{1 + TWV_{11}^{um} \times (\omega^2 m_{\text{acc}})} \tag{12}$$

This Eq. (12) can be used to compute the modified FRF system structure by coupling the original FRFs obtained from the accelerometer and its mass effect, clamped with the help of a vise, on the thin-wall workpieces with nominal thickness of 1, 2, 3, 4, and 5 mm.

The mass of the Kistler ultra-miniature accelerometers was measured by using an analytic balance to take into account the cable effects since it could add extra mass on the thin wall depending on the suspended cable length. We performed several measurements by bending cable upwards at different cable hanging lengths in order to achieve the configuration with the minimum mass effect, as shown in Fig. 4. In this case, the estimated added mass value varies from 0.5 to 0.6 g.

Figure 5 shows the FRF measurements using both the laser vibrometer and the accelerometer. Vibsoft package was used to obtain the corresponding displacement/force FRF from accelerometer and LDV measurements. In Fig. 5, the dashed black line represents the numerical results obtained by using Eq. (12) in which the FRF measured from the accelerometer was compensated to eliminate the added mass of 0.58 g due to the accelerometer and cable array. It is clear that the compensation method shifts the FRF signal to the higher frequencies with respect to the accelerometer measurements. With this shift, the modified signal matches the signal obtained from the vibrometer measurements (red solid line). This confirms that the mass compensation method can modify the accelerometer FRFs to take into account the effect of the added mass to the thin-wall workpiece. Similar to the calculation of the FRF to subtract the mass effects by using the modification method, the measured FRF with the added mass can be estimated from the driving point function $D_{11} = \Delta m = \omega m^2_{\text{acc}}$.

5 Compensation of the accelerometer cable damping effects

Based on the results obtained by using the structural modification method that shifted the FRFs measured signals to compensate the mass added to the system, we now focus our attention on deriving a similar scheme to consider damping effects that could be due to the accelerometer cable length. This step will provide accurate system modal parameter values that are needed to compute the cutting parameter values that will help us to determine a stable workpiece machining process by using either frequency [17] or time domain methods [18–20]. Since the usage of mini-accelerometers to acquire FRFs is common because of its lower cost compared to the vibrometer measurement system, we now focus our attention on compensating the FRF values obtained from an accelerometer with a standard cable attached to a workpiece with 4.8 mm wall thickness, 50 mm width, and 35 mm height. For this case, we used a mini-accelerometer Dytran 3225F1 of 0.6 g (see Fig. 4), and we have measured 1.24 g of mass that was added by the cable array. Figure 6 shows, in time domain, how the mini-accelerometer cable increases the damping in comparison to LDV measurements. To compensate the accelerometer and cable mass effects during the determination of the FRF experimental values, we have used the structural modification method described by Eq. (12). The accelerometer FRF and its modified FRF are plotted in Fig. 7. Notice that the accelerometer FRF compensation method eliminates the added mass; however, it cannot match the vibrometer FRF

Table 2 List of the modal parameter computed by using the laser vibrometer system and the accelerometer device

Modal parameters	Accelerometer			Laser Doppler vibrometer
	Without modifications	With mass compensation	With mass and damping compensation	
Frequency [Hz]	2518	2754	2759	2758
Damping ratio	0.0213	0.0237	0.0073	0.0079
Mass [kg]	0.0072	0.0076	0.0076	0.0076

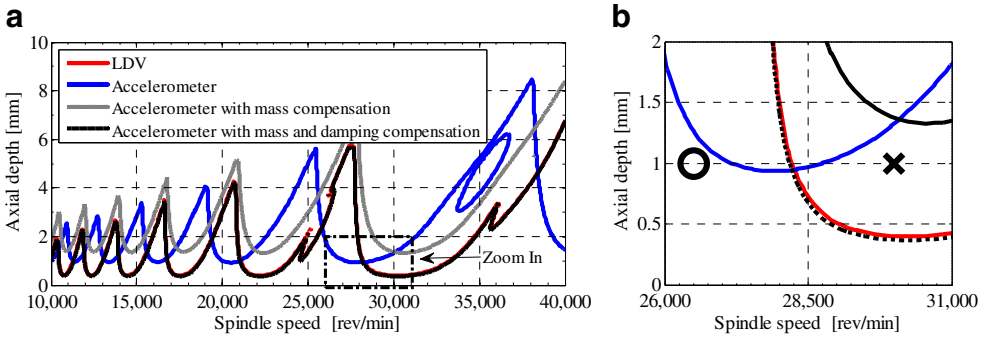

Fig. 8 **a**) Stability diagrams for a 4.8 mm thin wall machining, by using LDV, accelerometer, and mass-damping compensation FRFs. **b**) *Zoom in*, symbols *o* and *x* denote stable and unstable conditions, respectively

measurements because the peak oscillation amplitude has decreased. This is due to the extra damping added by the cable. In order to compensate this extra damping cable effects, we introduce here a damping compensation term $D_{11}=-\omega^2 m_{acc}+\omega c_{acc}$ in Eq. (9). By using the vibrometer FRF as a reference value, we have computed an estimated extra added damping value to the system of about $\Delta_{11}H=-4.3$ Ns/m. Figure 7 shows that the accelerometer FRF, with mass and damping compensation, closely match the vibrometer FRF curves. It is important to mention that the estimated extra added damping value is very sensitive to the cable setup i.e., to the hanging length and to the fastening position. Then, the same damping compensation value could be used for other walls if the cable configuration is duplicated.

In order to validate experimentally the influence of the accelerometer's mass and damping during the milling cutting operation of an aluminum block with 4.8 mm thickness, 50 mm width, and 35 mm height, both raw and modified accelerometer FRF measurements were used to compute the corresponding stability lobes by using the enhanced multi-stage homotopy perturbation method (EMHPM) [7]. Since the EMHPM is a time domain method, the modal parameters were fitted from the FRFs by using a commercial software CutPro 6.0. Table 2 lists the modal parameter values obtained by using the accelerometer and the laser vibrometer systems. Experimental machining tests were made in a Makino F3 milling center, with a carbide 0.5 in square end-mill tool with two 20° helix flutes, by considering a radial depth of cut of 0.8 mm and a spindle speed of 30,000 rpm. The cutting force coefficient values of $K_t=968$ N/mm^2 and $K_r=392$ N/mm^2 were estimated by using the procedure described in [21]. Down milling operation is chosen for this study because the thin wall tends to move away from the tool due to the action of the cutting force [14]. This allows us to obtain a wider stable zone at high-speed machining.

As we can see from the stability lobes showed in Fig. 8, the attachment of a 0.6 g accelerometer and a total mass of 1.24 g due to the hanging cable to a thin-wall workpiece strongly influences the stability boundaries. Therefore, if one considers the usage of accelerometer devices to determine the modal parameter values that will help to compute the cutting machine stability lobes, we could erroneously select machine parameter values that could produce unstable machine operation instead of having a stable one, as shown in Fig. 8.

Therefore, we can conclude that if we consider the damping and mass effects of the cable and the accelerometer, we could predict with accuracy LDV measurements. For instance, at 26,500 rpm, the accelerometer FRF and the accelerometer with mass and damping compensation predicts stable cutting conditions (frequency peaks match with multiples tool passing frequencies), as shown in Figs. 8 and 9a. However, at the spindle speed of 30,000 rpm, the modal data collected from accelerometer measurements predict stable cutting conditions, while the modified accelerometer FRF with mass and damping compensation predicts unstable behavior. This result agrees with experimental observations shown in Fig. 9b. In this case, the vibration amplitude recorded at 30,000 rpm is about 0.6 mm/s and the system exhibits quasi-periodic chatter frequencies (see Fig. 9b) which confirm an unstable milling process.

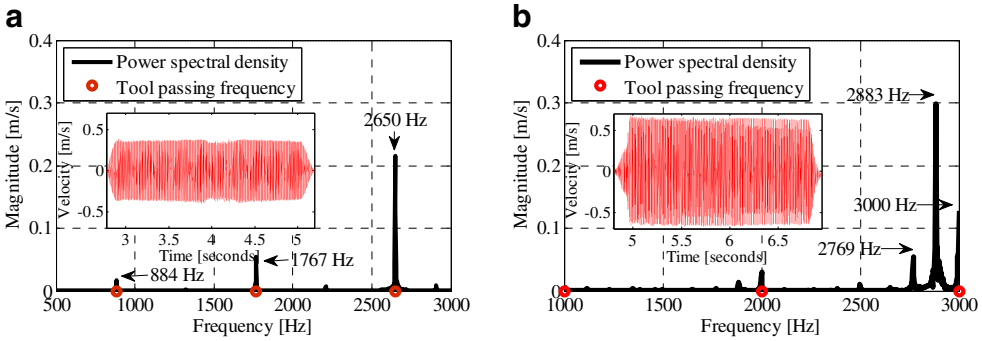

Fig. 9 Experimental data of **a**) stable cutting at 26,500 rpm and **b**) unstable cutting at 30,000 rpm

6 Conclusions

In this paper, we have found that an ultra-miniature 0.4 g accelerometer provides FRF signals that are different from those recorded by a vibrometer device. In fact, we have tested five thin-wall workpieces with different thicknesses and found that the measurements recorded from the laser vibrometer and the accelerometer device differ, as shown in Fig. 5. To correlate these discrepancies in the collected FRF values, we have applied the structural modification method that takes into account the mass accelerometer effects [16]. In fact, the original accelerometer FRF measurements are, by using Eq. (12), shifted to high frequencies. This confirms that this method can be used to fix the accelerometer FRF measurement to match with those obtained by using the laser vibrometer system.

During the process of determining stable milling cutting conditions, we also have found that stable cutting conditions predicted from the FRF accelerometer data disagree with physical observations, while the stable cutting conditions obtained from the laser vibrometer FRF data follow well with experimental data. These results show that the accelerometer's mass and the damping effects due to the connecting cable are causing deviations in stability boundaries. Based on these experimental observations, it is clear that if the cable damping effects are considered, then we can obtain stability bounds that agree with experimental observations. Therefore, we need to use a damping term to compensate the cable damping effects to match experimental data obtained via the LDV system.

Acknowledgments This work was funded by Tecnológico de Monterrey, Campus Monterrey, through the Research group of Nanotechnology and Devices Design and the Research group of Advanced Manufacturing. Additional support was provided by Consejo Nacional de Ciencia y Tecnología (CONACYT), Project Number 242269, México, and by Polytec Inc.

References

1. Altintas Y, Budak E (1995) Analytical prediction of stability lobes in milling. CIRP Ann Manuf Technol 44(1):357–362
2. Urbikain G, López de Lacalle LN, Fernández A (2014) Regenerative vibration avoidance due to tool tangential dynamics in interrupted turning operations. J Sound Vib 333(17):3996–4006
3. Campa FJ, Lopez de Lacalle LN, Celaya A (2011) Chatter avoidance in the milling of thin floors with bull-nose end mills: model and stability diagrams. Int J Mach Tools Manuf 51(1):43–53
4. Wan M, Murat Kilic Z, Altintas Y (2015) Mechanics and dynamics of multifunctional tools. J Manuf Sci Eng-T ASME 137(1):011019
5. Insperger T, Stepan G (2004) Updated semi-discretization method for periodic delay-differential equations with discrete delay. Int J Numer Methods Eng 61(1):117–141
6. Ding Y et al (2010) Second-order full-discretization method for milling stability prediction. Int J Mach Tools Manuf 50(10):926–932
7. Compeán FI et al (2012) Characterization and stability analysis of a multivariable milling tool by the enhanced multistage homotopy perturbation method. Int J Mach Tools Manuf 57:27–33
8. Butcher EA, Nindujarla P, Bueler E (2005) Stability of up- and down-milling using Chebyshev collocation method. Proc ASME Int Des Eng Tech Conf Comput Inf Eng Conf 6(Pts A-C):841–850
9. Sims ND, Bayly PV, Young KA (2005) Piezoelectric sensors and actuators for milling tool stability lobes. J Sound Vib 281(3–5):743–762
10. Castro LR, Vieville P, Lipinski P (2006) Correction of dynamic effects on force measurements made with piezoelectric dynamometers. Int J Mach Tools Manuf 46(14):1707–1715
11. Olvera D et al (2014) Determination of the stability lobes in milling operations based on homotopy and simulated annealing techniques. Mechatronics 24(3):177–185
12. Budak E, Altintas Y (1995) Modeling and avoidance of static form errors in peripheral milling of plates. Int J Mach Tools Manuf 35(3):459–476
13. Campa FJ (2009) A method to predict and avoid instabilities on the thin floors milling process. Dissertation, University of the Basque Country
14. Bravo U et al (2005) Stability limits of milling considering the flexibility of the workpiece and the machine. Int J Mach Tools Manuf 45(15):1669–1680
15. Özşahin O, Özgüven HN, Budak E (2010) Analysis and compensation of mass loading effect of accelerometers on tool point FRF measurements for chatter stability predictions. Int J Mach Tools Manuf 50(6):585–589
16. Nevzat Özgüven H (1990) Structural modifications using frequency response functions. Mech Syst Signal Process 4(1):53–63
17. Budak E, Altintas Y (1998) Analytical prediction of chatter stability in milling—part 1: general formulation. J Dyn Syst-T ASME 120(1):22–30
18. Bayly PV et al (2003) Stability of interrupted cutting by temporal finite element analysis. J Manuf Sci Eng-T ASME 125(2):220–225
19. Insperger T, Stepan G (2002) Semi-discretization method for delayed systems. Int J Numer Methods Eng 55(5):503–518
20. Ding Y et al (2010) A full-discretization method for prediction of milling stability. Int J Mach Tools Manuf 50(5):502–509
21. Altintas Y (2000) Manufacturing automation: metal cutting mechanics, machine tool vibrations, and CNC design. Cambridge University Press, New York